Journal of Power Sources 652 (2025) 237692

Contents lists available at ScienceDirect

Journal of Power Sources

journal homepage: www.elsevier.com/locate/jpowsour

Effect of operating conditions on Molten Carbonate Electrolysis Cell performance: an experimental study

Simone Mataloni [a,b,*], Silvia Lo Conte [b], Massimiliano Della Pietra [a], Francesca Santoni [a], Alfredo Zingone [a], Nicola Verdone [b]

[a] Department of Energy Technologies and Renewable Sources, Laboratory for Hydrogen and New Energy Vectors (TERIN-DEC-H2V), ENEA Italian National Agency for Energy, New Technologies and Sustainable Economic Development, R.C. Casaccia, Rome, Italy
[b] University of Rome "La Sapienza", Department of Chemical Engineering Materials and Environment, Via Eudossiana 18, 00184, Rome, Italy

HIGHLIGHTS

- MCEC tested under varying CO_2 and H_2O concentrations at different temperatures.
- Low CO_2 feeding enables pure H_2 production.
- rWGS reaction identified as key mechanism under water-limited conditions.
- Gas analysis confirms deviation from electrolysis-only predictions.
- Thermodynamic model shows rWGS potential exceeds experimental conversion.

ARTICLE INFO

Keywords:
Hydrogen production
Carbon utilization
Molten carbonate electrolysis cell
Concentration effect
Temperature effect
Gas analysis

ABSTRACT

The study investigates the performance of a Molten Carbonate Electrolysis Cell (MCEC) under varying operational conditions, focusing on the interplay between electrochemical reactions and reverse water-gas shift (rWGS) reaction. Experimental tests were conducted using a MCEC single repeating unit (100 cm^2 active area), operating at different temperatures (620 °C, 650 °C, and 680 °C) and varying feed compositions of H_2O and CO_2 (10 %, 20 %, 30 %, and 40 % molar fractions) at the fuel electrode. Electrochemical performance was evaluated through galvanostatic polarization and electrochemical impedance spectroscopy (EIS), while gas compositions were analyzed via gas chromatography to gain insights into the rate of reactions. Increasing operating temperature improves electrochemical performances while also enhancing the rWGS reaction, with a greater interplay between chemical and electrochemical processes. Higher CO_2 and H_2O concentrations influenced both electrolysis and rWGS, affecting overall cell performance. Notably, limited CO_2 supply led to performance degradation, indicating its crucial role not only as a reactant in electrolysis but also in sustaining rWGS. The study also observed that excess CO_2 contributed to maintaining cell efficiency by promoting rWGS, supplementing H_2 production under water-limited conditions. Findings can contribute to better understand the interactions between temperature, gas composition, and reaction mechanisms in MCECs, offering possibilities for optimization.

1. Introduction

In the scientific community, there is a growing urgency to develop technologies capable of significantly reducing CO_2 emissions, a crucial step toward achieving the European Commission's climate neutrality target by 2050 [1]. Particular attention is being given to "Hard-to-Abate" sectors, which present significant challenges due to the difficulty of electrification and the excessive costs associated with the transition. In 2022, global CO_2 emissions reached 36.8 Gt [2] with heat and electricity contributing 14.6 Gt, the highest level ever recorded [2]. Other productive industries emitted 9.15 Gt of CO_2 in 2022, accounting for 25 % of global emissions [2], with heavy industries (cement, iron and

* Corresponding author. Department of Energy Technologies and Renewable Sources, Laboratory for Hydrogen and New Energy Vectors (TERIN-DEC-H2V), ENEA Italian National Agency for Energy, New Technologies and Sustainable Economic Development, R.C. Casaccia, Rome, Italy.
E-mail address: simone.mataloni@enea.it (S. Mataloni).

https://doi.org/10.1016/j.jpowsour.2025.237692
Received 10 April 2025; Received in revised form 13 June 2025; Accepted 16 June 2025
Available online 19 June 2025

steel, chemical production) being among the most difficult to decarbonize [3]. Freight and passenger transport added 7.98 Gt of CO_2, representing 22 % of the global emissions, with around 20 % stemming from hard-to-electrify modes of transport, such as maritime shipping and aviation [2,4]. Therefore, advancing the energy transition in these sectors to reduce their carbon footprint is a primary goal for the near future.

At the same time, interest in hydrogen production is increasing across Europe and globally, driven by its potential applications in chemical production, energy storage, and fuel use.

In 2022, global hydrogen production reached nearly 95 Mt, marking an increase of 3 % compared to 2021 [5]. However, the majority of this production was still dominated by the unabated use of fossil fuels. Natural gas without carbon capture, utilization, and storage (CCUS) accounted for 62 % of global production, while unabated coal, primarily in China, contributed 21 %. By-product hydrogen, generated during naphtha reforming in refineries and the petrochemical industry, accounted for another 16 % of the total production. Only a small fraction (0.7 %) of hydrogen production came from renewable sources or fossil fuel technologies equipped with CCUS [5].

Reducing dependence on fossil fuels is crucial, and the implementation of high-efficiency processes, such as those that integrate renewable energy with CCUS, is essential to support the energy transition and meet growing hydrogen demand.

In this context, Molten Carbonate Electrolysis Cells (MCECs) offer a promising pathway for clean hydrogen production, as they facilitate both hydrogen generation and CO_2 capture in a single process.

MCECs, taking advantage of the co-electrolysis of H_2O and CO_2, represent an innovation in the scientific landscape as devices capable of converting electrical energy into green hydrogen while enabling the carbon dioxide sequestration. This technology is advantageous because it allows the co-electrolysis of water and CO_2 in a single device, improving overall efficiency compared to separate electrolysis processes. MCECs also offer the added benefit of producing syngas in a controllable H_2/CO ratio, which is ideal for the synthesis of fuels and chemicals [5,6].

Co-electrolysis has been extensively studied in Solid Oxide Electrolysis Cells (SOECs) as an innovative process to produce synthetic fuels and chemicals with low environmental impact. In these systems, water and CO_2 are simultaneously reduced in a single electrolytic unit using electricity, preferably from renewable sources. The main result is the production of syngas, a mixture of hydrogen (H_2) and carbon monoxide (CO), which can then be converted into liquid fuels such as methanol, dimethyl ether, or synthetic hydrocarbons via processes such as Fischer-Tropsch synthesis [7–9].

In MCEC, water and carbon dioxide are supplied to the fuel electrode, where the following electrochemical reactions occur:

$$\text{Fuel Electrode} : H_2O + CO_2 + 2e^- \rightleftharpoons H_2 + CO_3^{2-} \quad (1)$$

$$\text{Oxidant Electrode} : CO_3^{2-} \rightleftharpoons \frac{1}{2} O_2 + CO_2 + 2e^- \quad (2)$$

$$\text{Full Reaction} : H_2O + CO_{2,fe} \rightleftharpoons H2_{+}\frac{1}{2} O_2 + CO_{2,o}e \quad (3)$$

Molten carbonate cells operate at high temperatures, typically between 550 and 700 °C. These elevated temperatures help improve the overall energy efficiency of the process reducing the electrical energy required for electrochemical reactions, since some of the energy is delivered as heat [10].

At these temperatures, in addition to the primary electrochemical reactions, other chemical reactions can occur favored by operative conditions and the presence of the electrode catalysts. The principal reaction occurring is the Reverse Water Gas Shift Reaction (rWGS):

$$H_2 + CO_2 \rightleftharpoons H_2O + CO \quad (4)$$

Depending on the concentration of CO_2 and operating temperatures, this reaction can result in a higher or lower production of carbon monoxide, depleting reactants for the electrolysis and reducing the concentration of hydrogen leaving the cell.

To the authors' knowledge, numerous studies in literature focus on the operation of molten carbonate cells in fuel cell mode. These modeling and experimental works include research on both semi-ideal systems, such as Button cells, and on more easily scalable systems, such as single cells. Of particular importance in these terms are studies on process integration, by retrofitting or implementation, of molten carbonate devices for H_2 utilization and CO_2 capture [11–14], with an interesting insight into the field of emission control in heavy maritime transport [15–17]. Additionally, research has been conducted on the constituent materials of the cells [18,19] and their physio-chemical properties [20]. In the last years, works regarding electrolysis in molten carbonate cells have increased, including multidimensional modeling of electrolysers [21], experimental studies on transport phenomena, chemical and electrochemical reactions, and charge transfer mechanisms [22–25], and studies on cell reversibility [6,26–28].

Although the potential of MCECs for co-electrolysis of H_2O and CO_2 has been recognized in recent studies [29,30], especially for synthetic fuel generation [31,32], most research has focused on modeling approaches or limited electrochemical characterization. Experimental works that provide direct gas analysis under controlled operating conditions remain scarce and not fully applied to all gas species [33,34]. Furthermore, while the role of high-temperature co-electrolysis in syngas production is acknowledged, the interplay between electrochemical and thermochemical reactions, particularly the contribution of rWGS under varying feed conditions, is still not fully understood. Also is not directly demonstrated whether the carbon monoxide originates from electrochemical or chemical processes Our study contributes to this area by systematically exploring the effects of temperature and CO_2/H_2O feed ratio on cell performance and gas composition, with supporting electrochemical impedance, galvanostatic polarization and chromatographic data.

2. Experimental set-up

Investigating the working principles of MCEC technology applied to hydrogen production and carbon sequestration needs an experimental set-up that meets the objectives requirements. Considering this, the best solution is to experiment with Single Cell (SC) unit set-up, since those can provide experimental results suitable for industrial scalability purposes and allow obtaining valuable gas analysis data. Since the MCEC devices require specific equipment for the optimal control of temperature, gas flow and each gas volume fraction, water vapor flow, current density, it is of prior importance using a test bench that can provide a fine tuning of these parameters. For the purpose, it has been utilized a MCFC TEST STATION produced by CNL Energy CO. Ltd (Fig. 1).

The equipment provides a furnace capable of reaching the desired temperature of operation (around 650 °C) and is designed for an in-operando tuning of the temperature as well as monitoring the temperature of the cell itself with a stand-alone thermocouple. The gas flow directed to the electrodes is controlled by six Bronkhorst® EL-FLOW® Classic mass flow meters/controllers. For water vapor control to the fuel electrode, a humidifier has been used. The dry fraction (H_2, CO_2, N_2) of the gas flow passes through water kept at specific temperature and for each different water temperature corresponds to a vapor volume fraction in the outlet stream. The humidified gas mixture is maintained above the evaporation temperature by means of pipelines heated with electrical resistances set at 120 °C, ensuring that no water condenses before entering the cell. Moreover, the system has been previously validated through experimental tests to verify the actual amount of water delivered. The cell is housed within two stainless steel SS316 casing, placed inside the heating furnace, equipped with conduits for the supply of gases and water vapor to the electrodes. The casings also serve

Fig. 1. MCFC test station

as electrical connections from the furnace exterior to the cell itself. An electronic load (ELS300Z, ELTO DC Electronics Co.) was used to supply current and measure cell voltage.

The experimental data were obtained through an analysis of the performance of a SC unit with an active surface area of 100 cm^2. The materials and state-of-the-art data were provided by the Korean Institute of Science and Technology (KIST).

The cell tested is composed of two electrodes: the fuel electrode (FE) made of a Ni alloy with 5 $\%_{wt}$ Al and the oxidant electrode (OE) made of NiO. The electrodes are divided by the electrolyte, a eutectic mixture of 62/38 mol % Li_2CO_3/K_2CO_3. At the operating temperature of the cell (around 650 °C), the electrolyte is in a liquid phase. A porous matrix, made of γ-$LiAlO_2$, which not only retains the molten carbonate electrolyte but also acts as a physical and chemical barrier that prevents cross-diffusion of gases. The matrix provides ionic conductivity for carbonate ions while maintaining gas-tight separation between the fuel and oxidant electrodes, thereby preserving the integrity of the electrochemical environment. The electrolyte and matrix are provided in the form of soft tape-casted sheets hand cut to fit the shape of the casings (130 mm square); stacking them between the two casings enables electrode electrical separation as well as sealing the assembly for separating oxygen and fuel gases. These material choices were based on well-established MCC configurations [25,28], selected for their high stability and compatibility under high-temperature conditions. Importantly, all material parameters were kept constant throughout the campaign to ensure that the effects of temperature and gas composition on cell performance could be analyzed without the interference of material-dependent variables. During the experimental campaign, the cell assembly is kept sealed using an external pressure of 2 bar applied by an air piston.

An exhaustive representation of the casing-electrode-matrix-electrolyte assembly and material details are reported in Fig. 2 and Table 1.

3. Experimental campaign

To better understand the electrochemical performance of the molten carbonate electrolysis cell, two independent variations of the water vapor and carbon dioxide content respectively in the feed stream to the fuel electrode will be introduced. The rationale for investigating the effects of varying H_2O and CO_2 content stems from their differing diffusion properties through the porous nickel electrode, which directly influences performance variations in terms of Electrochemical Impedance Spectra and Polarization Curves [35]. The compositions to be analyzed have been defined as 10 %, 20 %, 30 %, and 40 % molar

Table 1
Specification of 100 cm^2 unit cell.

Single cell components	Specification	
Cell Casing	Size [mm x mm]	130 × 130
	Material	AISI 316 L
Anode	Size [mm x mm]	110 × 110
	Thickness [mm]	0.7
	Current Collector	Pure Ni
	Material	Ni + 5 % wt Al
	Porosity	55–60 %
Cathode	Size [mm x mm]	100 × 100
	Thickness [mm]	0.7
	Current Collector	AISI 316 L
	Material	NiO
	Porosity	60–65 %
Electrolyte Matrix	Material	Li_2CO_3/K_2CO_3
	Material	γ-$LiAlO_2$
	Thickness [mm]	1.2

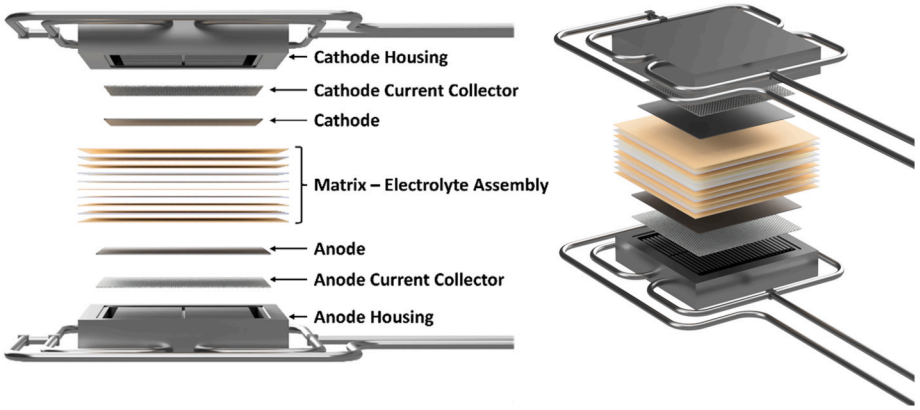

Fig. 2. MCEC assembly.

fraction of water vapor and 10 %, 20 %, 30 %, and 40 % molar fraction of CO_2. The feed stream to the fuel electrode will also be adjusted by modifying the partial pressure of N_2. This allows the mole fraction of the compound being studied to be varied without altering the fractions of the other components essential for the electrochemical reactions. All other mole fractions of the feed streams entering the cell will remain unchanged for the duration of the experiment, since the total flowrate has been kept constant. The parametric study will also address the variation of the operating temperature for investigating its effect on the chemical-physical characteristics of molten carbonate electrolysers.

Molten carbonate cells operate at temperatures above 500 °C, due to the need to have the electrolyte in the liquid phase. In fact, operating temperatures of liquid mixtures of Li and K carbonates are set in a range between 550 and 700 °C. Studies have identified 650 °C [13] as the optimal operating temperature for these devices.

The variation in operating temperature is of particular interest for evaluating the chemical-physical phenomena that take place in a molten carbonate cell. The temperature influences the diffusion processes of the components inside the device: an increase in temperature results in a greater molecular diffusion and a more homogeneous distribution of the compounds on the electrodes; on the contrary, a decrease would lead to a slowdown in diffusion processes. Furthermore, the temperature also affects the physical characteristics of electrical conductivity of the electrodes: the resistance of the anodic and cathodic metallic materials increases as the temperature decreases. No less important is the effect of temperature on the liquefaction condition of the electrolyte: higher temperature increases the ionic mobility within the matrix-electrolyte complex [36,37].

In the cell, Reaction 4 is favored by high operating temperatures; as the temperature varies, the reaction's favorability also changes, thereby influencing the consumption of reagents and the production of additional water vapor and carbon monoxide.

Tests will therefore be conducted at three different temperatures: 620 °C, 650 °C, and 680 °C, which represent a significant range for evaluating how the aforementioned phenomena influence the cell's performance. A too low temperature would significantly slow down the electrolysis reaction and reduce electrolyte conductivity [38], while a too high temperature could lead to rapid deterioration of the cell, due to fast electrolyte depletion [39] and increased current collectors corrosion [19]. A brief view of the different operating conditions studied and order of investigation is reported in Table 2.

For each combination of gas composition supplied to the fuel electrode at different temperatures, galvanostatic polarization (IV) tests and Electrochemical Impedance Spectroscopy (EIS) measurements were carried out. The EIS measurements were conducted using a Solartron SI-1260 frequency response analyzer module in conjunction with a Solartron SI-1287 Impedance/Gain-Phase analyzer. The impedance spectra were acquired by applying a 10 mV amplitude perturbation over a frequency range from 100,000 Hz–0.01 Hz, with a resolution of 10 points per decade to ensure a detailed characterization of the different electrochemical processes occurring within the cell. The EIS data were processed using ZView software for Windows, developed by Scribner Associates Inc.

In the Nyquist plots obtained, the spectra typically exhibit two distinct semicircles, which can be attributed to different physical and electrochemical phenomena within the system. The high-frequency semicircle is primarily associated with charge transfer resistance at the electrode/electrolyte interface, reflecting the kinetics of the electrochemical reactions occurring at the electrode surfaces. The low-frequency semicircle, on the other hand, is related to mass transport limitations, such as gas diffusion and the transport of reactants and products through the porous electrode and electrolyte matrix. Two parameters are considered in this work for comparing the behavior of different operative conditions: internal resistance (R_{int}) extracted as the intersection among the Nyquist plot and the x axis at high frequencies, and total resistance (R_{tot}) visualized as the low frequencies intersection. The R_{int} in MCEC systems typically refers to the impedance measured at frequencies below 1 kHz [40,41]. It encompasses various sources of resistance within the cell, such as limited ion mobility through the electrolyte confined in the matrix, imperfect electrical contact between adjacent materials, and restricted ionic transport within the porous structure of the electrodes.

The polarization curve is obtained by measuring the cell voltage as a function of the applied current density in galvanostatic mode. The initial voltage drop can be attributed to activation overpotential, linked to reaction kinetics. At intermediate currents, ohmic losses dominate, caused by resistance in electrodes, electrolyte, and contacts. At high currents, mass transport limitations lead to a sharp voltage drop due to reactant diffusion constraints. Analyzing the polarization curve helps identify limiting factors and optimize cell performance [35].

Following the determination of the polarization curve, measurements were taken at various current densities corresponding to different

Table 2
FE composition and temperature tested in the experimental campaign.

Type	Run	Fuel electrode		Oxidant electrode		T, °C
		Composition [%]	Flow rate [mL·min^{-1}]	Composition [%]	Flow rate [mL·min^{-1}]	
		$CO_2/H_2O/H_2/N_2$		$CO_2/O_2/N_2$		
Reference composition	1	20/20/10/50	400	30/15/55	400	**650**
H_2O variation	2	20/**10**/10/**60**	400	30/15/55	400	**650**
	3	20/**30**/10/**40**	400	30/15/55	400	**650**
	4	20/**40**/10/**30**	400	30/15/55	400	**650**
CO_2 variation	5	**10**/20/10/**60**	400	30/15/55	400	**650**
	6	**30**/20/10/**40**	400	30/15/55	400	**650**
	7	**40**/20/10/**30**	400	30/15/55	400	**650**
Reference composition	8	20/20/10/50	400	30/15/55	400	**620**
H_2O variation	9	20/**10**/10/**60**	400	30/15/55	400	**620**
	10	20/**30**/10/**40**	400	30/15/55	400	**620**
	11	20/**40**/10/**30**	400	30/15/55	400	**620**
CO_2 variation	12	**10**/20/10/**60**	400	30/15/55	400	**620**
	13	**30**/20/10/**40**	400	30/15/55	400	**620**
	14	**40**/20/10/**30**	400	30/15/55	400	**620**
Reference composition	15	20/20/10/50	400	30/15/55	400	**680**
H_2O variation	16	20/**10**/10/**60**	400	30/15/55	400	**680**
	17	20/**30**/10/**40**	400	30/15/55	400	**680**
	18	20/**40**/10/**30**	400	30/15/55	400	**680**
CO_2 variation	19	**10**/20/10/**60**	400	30/15/55	400	**680**
	20	**30**/20/10/**40**	400	30/15/55	400	**680**
	21	**40**/20/10/**30**	400	30/15/55	400	**680**

utilization factors, to quantify the hydrogen production through electrolysis and the CO formation. Keeping the cell under the chosen load conditions, gas chromatographic analyses were conducted on the outgoing streams from the hydrogen electrode.

The gas chromatography system used in this study is the Clarus 680 from PerkinElmer, equipped with specific columns for the targeted compounds, namely Haysep Q and Molecular Sieve 5A, along with a thermal conductivity detector (TCD) for optimal resolution. This instrument is capable of measuring H_2, CO, CO_2, N_2, as well as O_2 and CH_4, although the latter two are not of primary interest for this study. The gas sample was extracted directly from the outlet of the fuel electrode using a 1/16-inch stainless steel capillary probe connected to a micro diaphragm pump, ensuring a constant flow rate of 10 mL/min. To prevent condensation or adsorption of reactive species, the transfer line to the GC consisted of heated stainless steel tubing, maintained at approximately 120–150 °C and kept as short as possible. This setup ensured accurate and representative detection of the outlet gas composition.

4. Results

Before starting the main experiments, the MCC assembly underwent a pretreatment phase to reach the target operating temperature of 650 °C [42]. To ensure consistency and reliability in performance evaluation, the cell was initially tested using a **standard gas composition**, commonly used to validate MCFC operation [43]. This setup included a FE gas mixture of 72 % H_2, 18 % CO_2 and 10 % H_2O vapor with a total flow rate of 395.8 mL min^{-1}, whereas the OE was supplied with 15 % O_2, 55 % N_2 and 30 % CO_2 at a total flowrate of 951.0 mL min^{-1}.

This initial operating condition serves multiple purposes: it verifies the correct assembly of the cell, ensures that the electrochemical processes are stable before varying the experimental conditions, and most importantly allows for a direct comparison with previous and future tests using the same materials. By maintaining this reference point, we can better assess how different parameters influence performance.

4.1. Electrochemical stability and performance evaluation

The experimental campaign lasted for around 984 h, in which each of the different gas compositions and temperatures were tested. Since the extended duration of the experiments and the stressful conditions imposed, constant monitoring of the electrochemical stability of the cell was of primary importance. No electrolyte refilling was required during the entire experimental campaign. The cell was preserved by limiting exposure to potentially stressful conditions (e.g. high water concentrations) strictly to the time needed for stabilization and the execution of electrochemical and gas chromatographic tests. For the remaining periods, the system was maintained under reference conditions. Since the goal was not long-term durability testing but rather the exploration of a wide range of operating configurations, the experimental campaign was carefully designed to maximize the device's operational lifetime. For this purpose, polarization curves and EIS spectra were recorded periodically under specified conditions (in reference condition at 650 °C, see Table 2). The comparison of EIS spectra and IV curves measured at the start and end of the experimental campaign under these conditions is reported in Fig. 3. The open-circuit voltage and the voltage recorded at 10 A are respectively 0.965 V and 1.221 V for the beginning of the experimental campaign and 0.957 V and 1.226 V at the end. In terms of the EIS spectra, the internal resistance (R_{int}) and total resistance (R_{tot}) were at the start 0.41 Ω cm^2 and 2.4 Ω cm^2 and at the end 0.42 Ω cm^2 and 2.41 Ω cm^2, respectively. As shown in Fig. 3, findings indicate stable electrochemical behavior, suggesting that the MCEC maintained its operational integrity throughout the experimental period and no degradation occurred. Consequently, the authors assume the validity and comparability of the experimental data, as no significant changes in performance values were observed.

4.2. Temperature variation

To better investigate the chemical and electrochemical behavior of the cell, an in-depth analysis of temperature variation was performed. Fig. 4 present both EIS spectra and polarization curves at the three tested temperatures for three selected condition: Reference, 40 % CO_2 and 40 % H_2O. Table 3 lists the experimental values obtained in those aforementioned conditions.

The figures and Table 3 show that cell overpotential at 680 °C is lower than at both 620 °C and 650 °C for the same current densities. This confirms that operating at higher temperatures enhances electrochemical efficiency, primarily due to increased ionic mobility and decreased internal resistance [44,45]. However, it is important to note that the rWGS reaction is also more favorable at higher temperatures [46], impacting the overall gas composition at the hydrogen electrode and, in turn, the hydrogen yield. Therefore, while the results in Fig. 4 suggest that steam electrolysis in molten carbonate cells is favored at high temperatures, this must be evaluated in conjunction with the gas chromatography results presented later.

These findings are also reflected in the EIS measurements shown in the figure, where R_{int} decreases slightly with increasing temperature, while R_{tot} shows a more substantial reduction, indicating an overall improvement in charge transfer and mass transport phenomena. This consistency between polarization curves and impedance spectra further reinforces the importance of temperature as a key factor in defining MCEC performance.

4.3. Gas composition variation

To report the effects of varying the concentrations of gases supplied to the FE on electrochemical performance, data at the temperature of 650 °C were selected for presentation. The chemical and electrochemical behavior of the cell was experimentally observed at different temperatures. Nevertheless, presenting the results for the various temperatures does not substantially enhance the discussion beyond the analysis already provided for 650 °C.

From the analysis of the data presented in Fig. 5, summarized and

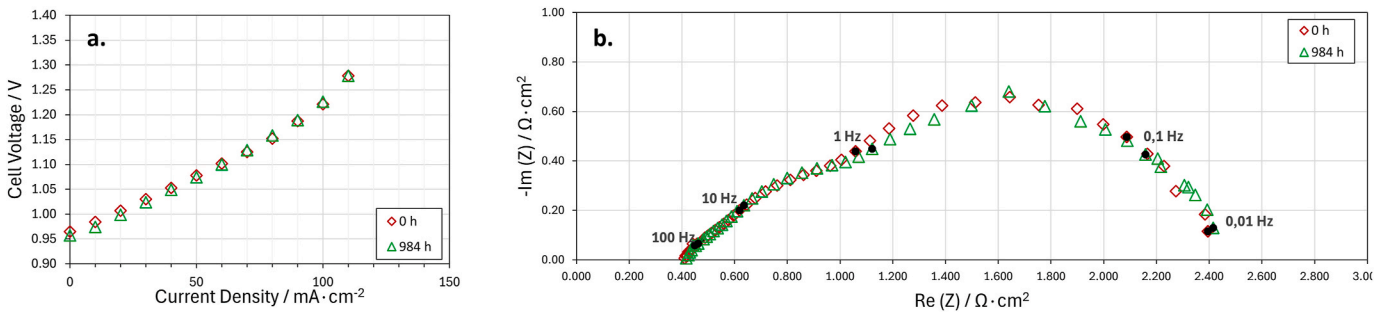

Fig. 3. *Electrochemical data at the start and end of the experimental campaign obtained at 650°C with reference composition:* **a.** *polarization curves;* **b.** *EIS spectra.*

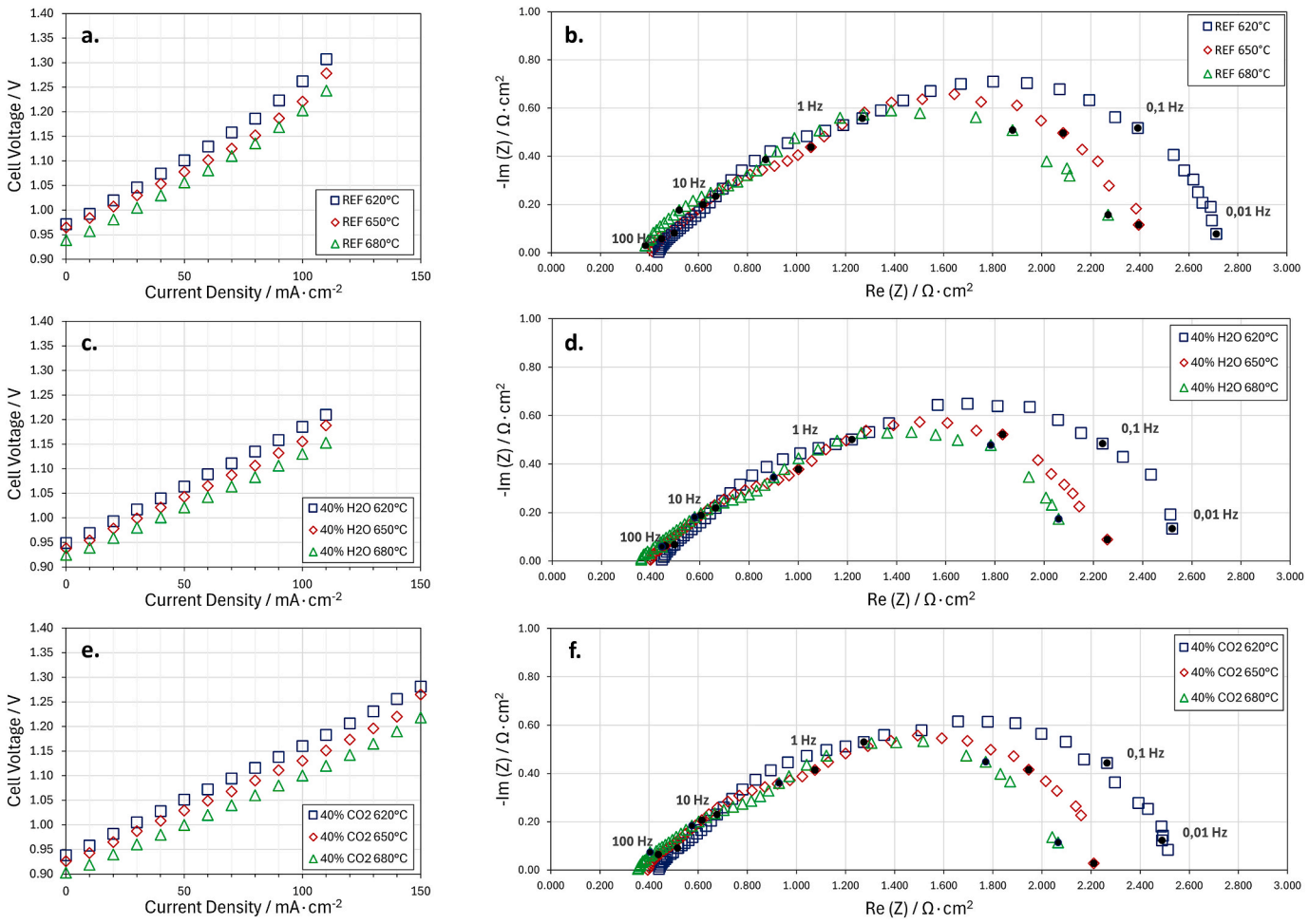

Fig. 4. *Temperature variation (620°C, 650°C, 680°C):* **a.** *Reference condition polarization curves;* **b.** *Reference condition EIS spectra;* **c.** *40 % H2O condition polarization curves;* **d.** *40 % H2O condition EIS spectra;* **e.** *Reference condition polarization curves;* **f.** *40 % CO2 condition EIS spectra.*

Table 3
EIS and IV data variation with temperature.

		620 °C	650 °C	680 °C	Measure Unit
Reference composition	R_{int}	0.44	0.41	0.38	Ω•cm^2
	R_{tot}	2.7	2.4	2.3	Ω•cm^2
	OCV	0.971	0.965	0.939	V
	ΔV (0–100 mA/cm^2)	0.291	0.275	0.264	V
40 % H_2O	R_{int}	0.45	0.40	0.36	Ω•cm^2
	R_{tot}	2.5	2.3	2.1	Ω•cm^2
	OCV	0.949	0.938	0.925	V
	ΔV (0–100 mA/cm^2)	0.236	0.217	0.205	V
40 % CO_2	R_{int}	0.44	0.40	0.35	Ω•cm^2
	R_{tot}	2.5	2.2	2.1	Ω•cm^2
	OCV	0.938	0.926	0.903	V
	ΔV (0–100 mA/cm^2)	0.222	0.204	0.197	V

highlighted in Table 4, it can be inferred that, in general, as the concentration of both gases necessary for co-electrolysis increase, the cell's performance improves accordingly. It is well known that a sufficient supply of reactants favors the electrochemical reaction [47].

It is particularly interesting to note that a limited supply of CO_2 leads to a significant deterioration in performance (Fig. 5, CO_2 variation, blue square markers), with a considerable increase in both OCV (0.998 V) and R_{tot} (2.8 Ω cm^2) compared to all other cases studied. This phenomenon, combined with the reduction in carbon dioxide content due to Reaction 4, suggests that CO_2 may be the limiting component for the electrochemical reactions in a MCEC.

Considering the results at 30–40 % CO_2 and 20 % H_2O, where water is theoretically the limiting reactant, the maximum current for electrolysis should be around 10 A, according to Faraday law of electrolysis:

$$r = \frac{I}{n_e \cdot F} \tag{5}$$

The reaction rate r defines the amount of gas transformed inside the cell as the current I varies, n_e is the number of electrons involved in Reaction 2 and F denotes the Faraday's constant. Specifically, it predicts the maximum theoretical amount of water vapor and carbon dioxide consumed, as well as the hydrogen produced, and the CO_2 transported to the OE. At 10 A of current supply, the reaction rate is 76.02 mL min^{-1}, which is slightly lower than the amount of water supplied to the cell (20 % i.e. 80 mL min^{-1}), and therefore at this current the water utilization factor would be close to 100 %. However, as shown in Fig. 5c, it is possible to apply even higher currents, reaching up to 150 mA/cm^2 for the case with 40 % CO_2. Thus, it is possible to achieve current densities higher than those predicted by Faraday's law and higher than those achievable in the reverse scenario, where the water content is 40 %. In this latter case, while it is still possible to exceed the 100 mA/cm^2 limit (see Fig. 5a), the slope of the polarization curve increases significantly at higher current densities, indicating a shortage of reactants in the cell.

A possible explanation for this phenomenon is that at high CO_2 concentrations, the system can exceed the theoretical reaction rate (r)

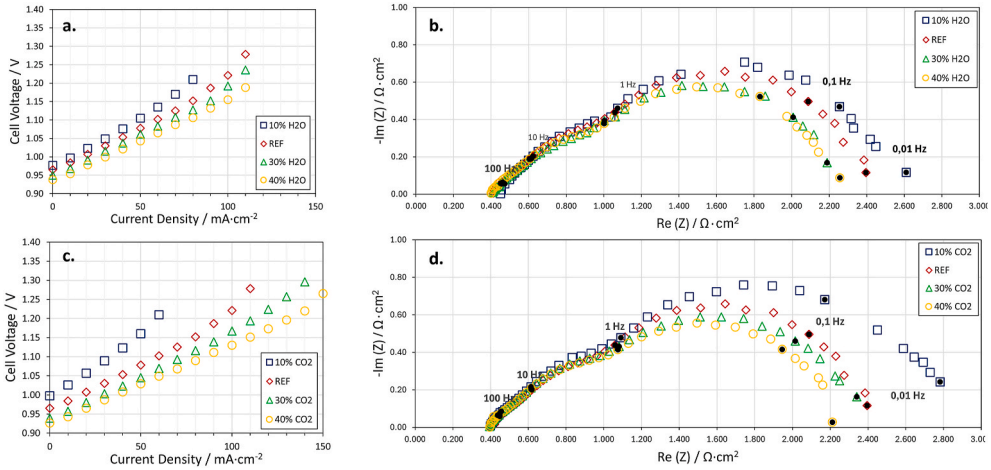

Fig. 5. *Concentration variation at 650 °C:* **a.** *H_2O variation polarization curves;* **b.** *H_2O variation EIS spectra;* **c.** *CO_2 variation polarization curves;* **d.** *CO_2 variation EIS spectra.*

Table 4
Experimental data illustrating the effects of H_2O and CO_2 concentrations (10 %, 30 %, and 40 %) on EIS spectra and polarization curves at 650 °C.

		10 %	30 %	40 %	Measure Unit
H_2O variation	R_{int}	0.44	0.40	0.45	Ω•cm^2
	R_{tot}	2.6	2.4	2.3	Ω•cm^2
	OCV	0.977	0.95	0.938	V
CO_2 variation	R_{int}	0.40	0.39	0.40	Ω•cm^2
	R_{tot}	2.8	2.3	2.2	Ω•cm^2
	OCV	0.998	0.939	0.926	V

because the reverse water-gas shift reaction (Reaction 4) generates additional H_2O, which can then participate in electrolysis, sustaining hydrogen production. An alternative hypothesis could be that the electrochemical performance is maintained by the direct electrolysis of CO_2:

$$2CO_2 + 2e^- \rightarrow CO + CO_3^{2-} \quad (6)$$

Since this reaction has been demonstrated to be highly hindered under typical MCEC operating conditions [27,29,33], the contribution of direct CO_2 electrolysis to CO production is likely negligible compared to the rWGS reaction. This hypothesis will be validated through gas analysis results.

4.4. Gas analysis

To analyze the composition of the gases exiting the cell, a gas chromatograph was used, as described in paragraph 2.3. Before conducting the analyses, the polarization curve was determined for each composition and temperature. Based on this, constant values of current density were selected for the composition study. The selected current densities were initially chosen arbitrarily but subsequently refined to focus on those at which the cell showed stable operation, as detailed earlier in the text. Data were generally collected at the FE in OCV, at 5A and 10A; measurements were also conducted at 15A for high CO_2 concentrations, as this condition enabled stable operation at higher current values.

It is important to note that gas chromatographs often struggle to accurately determine the volumetric fraction of water vapor. Typically, this fraction is calculated as the difference between the estimated total volume entering the system and the volume measured by the analysis columns. However, this method is delicate and frequently yields unreliable results. Therefore, to guarantee clarity in data presentation, the volumetric fractions reported by the gas chromatograph were provided on a dry basis, excluding the water vapor fraction. In order to compare the experimental results with the theoretical gas production/consumption, the gas chromatography data were used to evaluate the corresponding experimental outlet flowrates. The theoretical dry outlet flowrate was determined for each applied current by subtracting the electrolysis reaction rate and the outlet water flowrate, both calculated using Faraday's law, from the inlet flowrate (see eq. (10)). The experimental outlet flowrates were then calculated by multiplying the dry molar fractions measured by the gas chromatograph by this theoretical dry outlet flowrate.

As shown in Equations (7) and (8), theoretical gas flow rates were determined by adding the reaction rate (r) contribution to the incoming H_2 and subtracting it from the H_2O and CO_2 values. The electrolysis flow rate results in the amount entering the cell diminished by the r. These calculations were performed on a dry basis for consistency with the chromatographic data:

$$H_2 : F_{el,H2} = F_{in,H2} + r \quad (7)$$

$$H_2O \text{ and } CO_2 : F_{el,j} = F_{in,j} - r \quad (8)$$

$$\text{Electrolysis Flow Rate} : F_{el} = F_{in} - r \quad (9)$$

$$\text{Dry Final Flow Rate} : F_{el,dry} = F_{in} - F_{el,H2O} - r \quad (10)$$

Both experimental and calculated theoretical data are available for comparison in Table 5 and shown in Figs. 6–8.

Fig. 6 illustrates the behavior of the gases exiting the FE with a current supply of 5A at 650 °C. The graphs show the production and consumption trends of each component. In particular, CO flowrate decreases as the percentage of water vapor in the feed increases. Since both CO and H_2O are products of the rWGS reaction, an increase in water would inhibit the reaction. Conversely, for CO_2 variations, it can be observed that H_2 flowrate decreases as the CO_2 content in the inlet increases, further suggesting the significant role of rWGS under the analyzed conditions.

Interestingly, when the cell is fed with 10 % CO_2, no detectable amounts of CO or unreacted CO_2 are found in the hydrogen electrode exhaust. This suggests that, under certain conditions, the entire CO_2 supply is converted into carbonate ions and transported to the oxygen electrode. As a result, the gas stream at the hydrogen electrode consists solely of hydrogen and water vapor. Since water can be easily removed through condensation, the MCEC process not only enables CO_2 sequestration at the oxygen electrode but also facilitates the production of high-purity hydrogen.

By further comparing the 5A graphs in Fig. 6 with the 10A graphs in Fig. 7, it can be observed in all configurations that the flowrate of H_2

Table 5
Processed gas flowrates for different compositions, power supply and temperature: Experimental vs Theoretical data.

Applied current [A]	Gas Composition	T [°C]	Experimental Flowrate [mL·min^{-1}]			Theoretical Flowrate [mL·min^{-1}]			Electrolysis + rWGS Flowrate [mL·min-1]		
			H_2	CO_2	CO	H_2	CO_2	CO	H_2	CO_2	CO
5	REF	650	94.8	44.2	9.3	93.3	52.8	0.0	75.0	34.5	18.3
	10 % H_2O	650	99.0	44.2	10.8	93.3	52.8	0.0	66.9	26.3	26.4
	30 % H_2O	650	104.4	46.7	3.6	93.3	52.8	0.0	79.5	39	13.8
	40 % H_2O	650	100.5	50.2	4.6	93.3	52.8	0.0	82.3	41.8	11
	10 % CO_2	650	111.4	0.0	0.0	93.3	7.1	0.0	90.1	3.9	3.2
	30 % CO_2	650	92.8	84.5	16.2	93.3	98.5	0.0	65.1	70.2	28.2
	40 % CO_2	650	83.3	136.3	22.3	93.3	144.2	0.0	57.8	108.7	35.5
10	REF	650	138.2	1.9	9.2	131.3	14.8	0.0	120.9	4.4	10.4
	30 % H_2O	650	149.1	8.6	1.6	131.3	14.8	0.0	124.3	7.7	7
	40 % H_2O	650	148.4	9.1	1.0	131.3	14.8	0.0	126.1	9.5	5.3
	30 % CO_2	650	134.5	40.5	20.2	131.3	60.5	0.0	100.0	29.2	31.3
	40 % CO_2	650	124.7	84.8	30.8	131.3	106.2	0.0	86.8	61.7	44.5
15	40 % CO_2	620	161.6	38.9	25.1	169.3	68.2	0.0	122.9	21.8	46.4
	40 % CO_2	650	157.5	31.4	32.8	169.3	68.2	0.0	121.6	20.5	47.7
	40 % CO_2	680	152.5	26.1	42.3	169.3	68.2	0.0	120.4	19.2	48.9

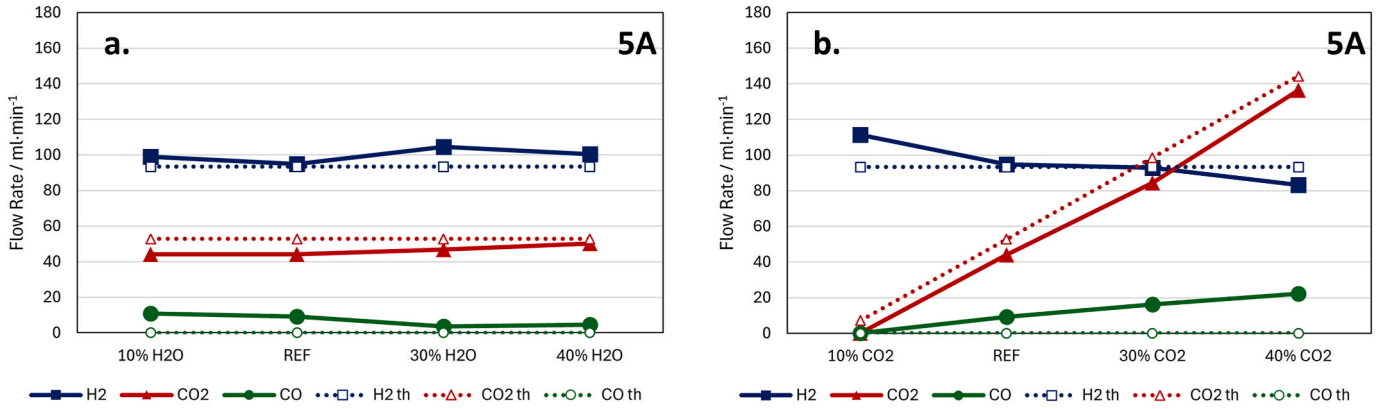

Fig. 6. Comparison among experimental flowrates estimated from gas chromatography data and Faraday's law theoretical data. Collected and calculated with a current supply of 5A at 650 °C: **a.** H_2O variation **b.** CO_2 variation.

produced increases significantly, correlating with a decrease in CO_2, while the CO flowrate remains nearly unchanged. For example, at 30 % CO_2, increasing the current from 5A to 10A raises the H_2 output from approximately 93 to 134 mL min^{-1}, while CO_2 drops from 85 to 41 mL min^{-1}. Meanwhile, CO output remains stable around 16 ÷ 20 mL min^{-1}. This supports the role of the rWGS reaction, as the stable CO levels suggest that the observed gas evolution is unlikely to stem from electrochemical processes.

The results obtained under specific operating conditions were then selected to distinguish between electrochemical and chemical contributions to gas evolution. In particular, the data obtained at 10A with 30 % and 40 % CO_2 (Fig. 7) and 15A with 40 % CO_2 (Fig. 8) were considered, as these conditions are relevant to the previous discussion on whether electrolysis can continue even after the complete consumption of the incoming water vapor. The results show that the amount of CO_2 exiting the cell is consistently lower than the theoretical value, suggesting that part of it is converted into CO through the rWGS reaction, producing an equivalent amount of carbon monoxide. To further support this interpretation, a thermodynamic calculation of the reverse water-gas shift (rWGS) equilibrium composition was performed using an equilibrium constant (K_e) of 0.51 at 650 °C [48]. As an illustrative case, we considered the experimental condition at 10 A with 40 % CO_2 at the fuel electrode. Based on the known inlet composition, temperature (650 °C), and assuming ideal gas behavior, the final equilibrium concentrations of H_2, CO, H_2O, and CO_2 were calculated by solving the equilibrium expression of the rWGS imposing CO flow rate (F_{CO}) as the unknown variable:

$$\text{rWGS Equilibrium}: K_e = \frac{\left(\frac{F_{out,H2O}}{F_{el}}\right)\left(\frac{F_{CO}}{F_{el}}\right)}{\left(\frac{F_{out,H2}}{F_{el}}\right)\left(\frac{F_{out,CO2}}{F_{el}}\right)} \quad (11)$$

$$\text{Final } H_2O \text{ flowrate}: F_{out,H2O} = F_{el,H2O} + F_{CO} \quad (12)$$

$$\text{Final } H_2 \text{ flowrate}: F_{out,H2} = F_{el,H2} - F_{CO} \quad (13)$$

$$\text{Final } CO_2 \text{ flowrate}: F_{out,CO2} = F_{el,CO2} - F_{CO} \quad (14)$$

The final results are showed in Fig. 7c and d. Also a full overview of the theorical data comprehending both electrolysis and rWGS are shown in Table 5.

The calculated composition shows a significantly higher conversion of CO_2 and H_2 to CO compared to our experimental data, indicating that the reaction is thermodynamically favorable under the investigated conditions. This confirms that the thermodynamic potential exists for the rWGS reaction to proceed further, and that the actual experimental gas composition is kinetically limited, not constrained by equilibrium. Therefore, the reaction rate is operating below the equilibrium conversion, possibly due to limited residence time, mass transport effects, or insufficient catalytic activation at the tested current density.

The temperature dependence of the rWGS reaction is further demonstrated by analyzing gas evolution between 620 °C and 680 °C (Fig. 8). As the temperature increases, the CO flowrate rises significantly from approximately 25 mL min^{-1} at 620 °C to nearly 42 mL min^{-1} at 680 °C, while both H_2 and CO_2 flowrates decrease from 162 to 152 mL

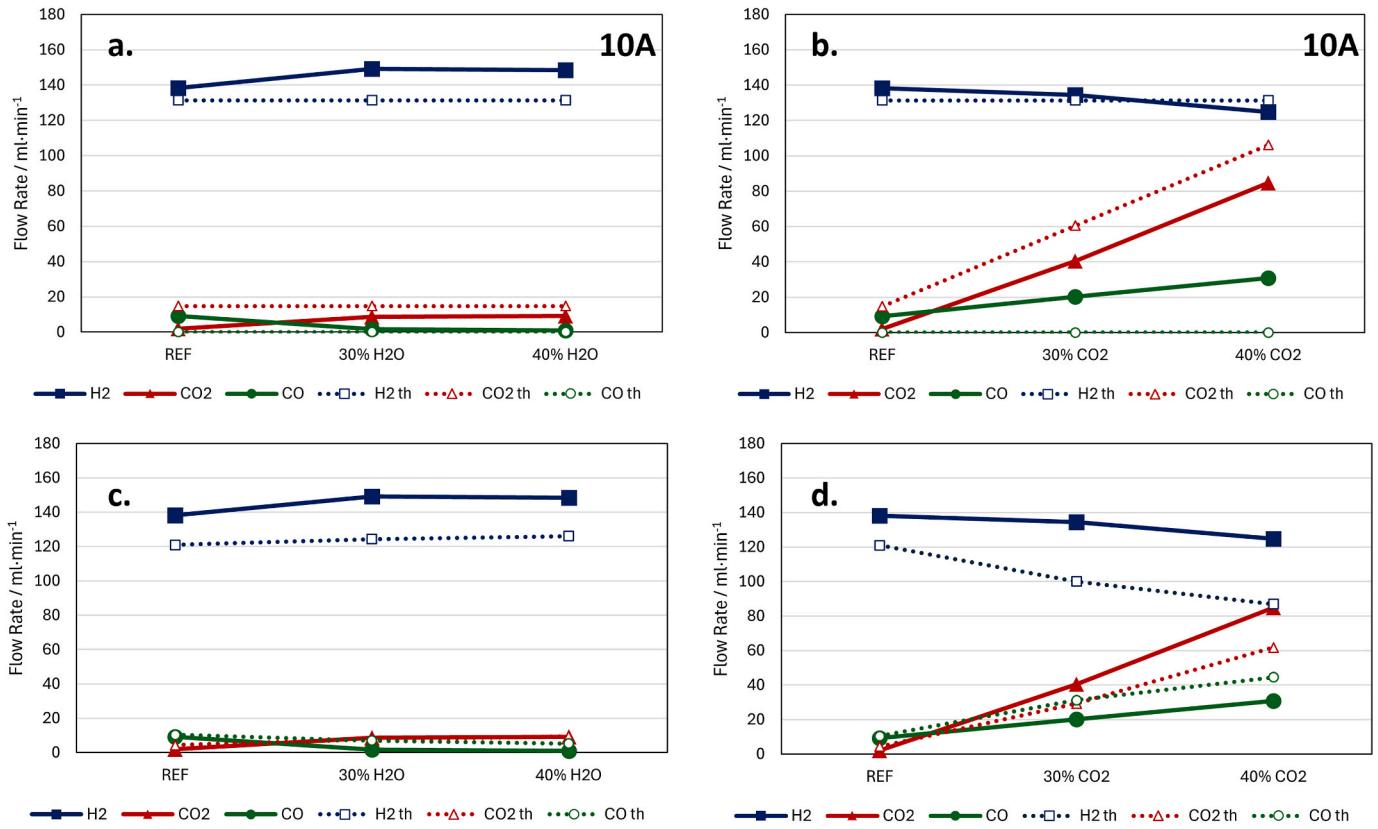

Fig. 7. *Comparison among gas chromatography data and theoretical data. Collected and calculated with a current supply of 10A at 650 °C:* **a.** *H_2O variation – Faraday's Law only;* **b.** *CO_2 variation– Faraday's Law only;* **c.** *H_2O variation – Faraday's Law and rWGS at equilibrium;* **d.** *CO_2 variation– Faraday's Law and rWGS at equilibrium.*

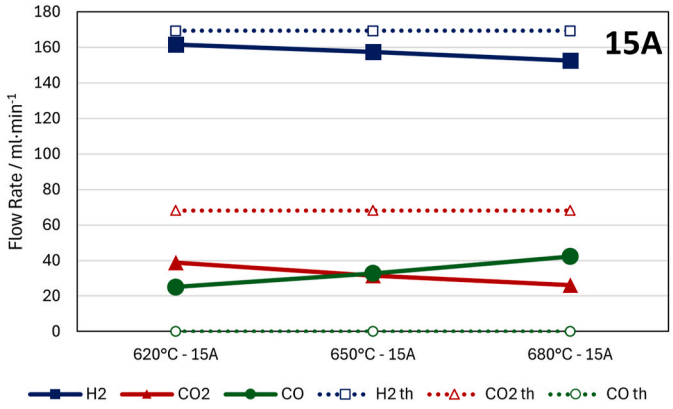

Fig. 8. 40 % concentration of CO_2 with a current supply of 15 A at 620 °C, 650 °C and 680 °C comparison among gas chromatography data and Faraday's law theoretical data.

min^{-1} and from 39 to 26 mL min^{-1} respectively. This is consistent with the endothermic nature of the rWGS reaction, which is thermodynamically favored at higher temperatures. The observed trends suggest that the reaction equilibrium progressively shifts toward CO and H_2O production, enhancing CO_2 conversion.

Moreover, increasing the CO_2 inlet concentration also promotes the reaction. At 650 °C and 10A (Fig. 7), an increase in CO_2 feed from 30 % to 40 % results in a CO increase from 20 to 31 mL min^{-1}. This indicates a higher conversion efficiency when more CO_2 is available. Notably, CO flowrate shows minimal variation with increasing current, reinforcing that its formation is governed by chemical rather than Faradaic reactions. At 40 % CO_2 and 650 °C, CO remains stable around 30 ÷ 32 mL min^{-1} across 10A and 15A, supporting the conclusion that rWGS is favored under these conditions.

Altogether, the combined impact of temperature, feed composition, and current highlights the strong dependence of the rWGS reaction on thermal and chemical parameters, highlighting the influence among chemical and electrochemical processes on each other performances. These trends not only support its dominant role in determining gas composition but also suggest opportunities for optimizing syngas output and CO_2 utilization through thermal and composition control strategies in MCEC systems.

5. Conclusions

This experimental study aimed to investigate the impact of operating conditions, particularly temperature and gas feed composition, on the performance of molten carbonate electrolysis cells. The results demonstrate that these factors significantly influence the cell's electrochemical behavior and overall efficiency. It was found that increasing the operating temperature enhanced electrochemical performance by improving ionic conductivity and mass transport, while simultaneously reducing internal and total cell resistances. A higher supply of CO_2 and H_2O improved reaction kinetics, leading to better hydrogen production and carbon dioxide utilization. However, performance deterioration was observed when CO_2 supply was insufficient, confirming its crucial role in sustaining the co-electrolysis process. Nevertheless, at low CO_2 feeding concentrations, corresponding to CO_2/H_2O molar ratios below 0.5, the cell exhibited the ability to produce high-purity hydrogen, as no CO or unconverted CO_2 were detected at the fuel electrode outlet. Furthermore, at CO_2/H_2O molar ratios between 1 and 2, because of the rWGS influence, is possible to increase carbon dioxide utilization and internal water recycling. Based on this, the reverse water-gas shift reaction was identified as a key secondary reaction that enhances hydrogen output under water-limited conditions. Gas chromatographic analysis

supported these findings. Experimental data were used to evaluate outlet flowrates that have been compared with theoretical predictions based on Faraday's law. In particular, under high CO_2 content and elevated currents, the experimental hydrogen and carbon dioxide output was consistently lower than the theoretical value predicted for electrolysis alone. This discrepancy further supports the concurrent occurrence of the reverse water-gas shift reaction alongside water electrolysis. These results highlight the potential of MCECs for scalable hydrogen production and carbon dioxide utilization. Future work should focus on quantifying hydrogen and carbon monoxide yields, followed by investigating system integration and long-term operational stability to ensure reliable and efficient performance in large-scale applications.

CRediT authorship contribution statement

Simone Mataloni: Writing – original draft, Visualization, Validation, Investigation, Formal analysis, Data curation. **Silvia Lo Conte:** Writing – review & editing, Validation, Investigation, Data curation. **Massimiliano Della Pietra:** Writing – review & editing, Supervision, Project administration, Methodology, Funding acquisition, Conceptualization. **Francesca Santoni:** Writing – review & editing, Resources, Investigation. **Alfredo Zingone:** Resources. **Nicola Verdone:** Writing – review & editing, Supervision.

Declaration of competing interest

The authors declare that they have no known competing financial interests or personal relationships that could have appeared to influence the work reported in this paper.

Acknowledgments

This research was funded by the European Union - NextGenerationEU from the Italian Ministry of Environment and Energy Security, POR H2 AdP MEES/ENEA with involvement of CNR and RSE, PNRR - Mission 2, Component 2, Investment 3.5 ″Ricerca e sviluppo sull'idrogeno", CUP: I83C22001170006.

Data availability

Data will be made available on request.

References

[1] European Commission, "2050 long-term strategy.," Clim. Action. [Online]. Available: https://climate.ec.europa.eu/eu-action/climate-strategies-targets/2050-long-term-strategy.
[2] IEA – International Energy Agency, "CO2 Emissions in 2022.," IEA publications - flagship report. [Online]. Available: https://www.iea.org/reports/co2-emissions-in-2022.
[3] IEA – International Energy Agency, "Transforming industry through CCUS.," IEA publications - technology report. [Online]. Available: https://www.iea.org/reports/transforming-industry-through-ccus.
[4] IEA – International Energy Agency, "Transport. Sectoral Overview," sectoral overview - tracking report. [Online]. Available: https://www.iea.org/reports/transport.
[5] Enea, "MCEC, a Promising, Innovative and Versatile Technology", doi: 10.12910/EAI2021-016.
[6] L. Hu, I. Rexed, G. Lindbergh, C. Lagergren, Electrochemical performance of reversible molten carbonate fuel cells, in: International Journal of Hydrogen Energy, Elsevier Ltd, Aug. 2014, pp. 12323–12329, https://doi.org/10.1016/j.ijhydene.2014.02.144.
[7] Y. Wang, T. Liu, L. Lei, F. Chen, High Temperature Solid Oxide H2O/CO2 co-electrolysis for Syngas Production, Elsevier B.V., 2017, https://doi.org/10.1016/j.fuproc.2016.08.009.
[8] W. Li, H. Wang, Y. Shi, N. Cai, Performance and methane production characteristics of H2O- CO2 co-electrolysis in solid oxide electrolysis cells, in: International Journal of Hydrogen Energy, Elsevier Ltd, Aug. 2013, pp. 11104–11109, https://doi.org/10.1016/j.ijhydene.2013.01.008.
[9] J. Aicart, M. Petitjean, J. Laurencin, L. Tallobre, L. Dessemond, Accurate predictions of H2O and CO2 co-electrolysis outlet compositions in operation, Int. J. Hydrogen Energy 40 (8) (Mar. 2015) 3134–3148, https://doi.org/10.1016/j.ijhydene.2015.01.031.
[10] R. Bove, A. Moreno, S. Mcphail, International status of molten Carbonate Fuel Cell (MCFC) technology [Online]. Available: http://ie.jrc.ec.europa.eu/, 2008.
[11] A. Monforti Ferrario, et al., A system integration analysis of a molten carbonate electrolysis cell as an off-gas recovery system in a steam-reforming process of an oil refinery, Front. Energy Res. 9 (Apr) (2021), https://doi.org/10.3389/fenrg.2021.655915.
[12] I. Rexed, M. della Pietra, S. McPhail, G. Lindbergh, C. Lagergren, Molten carbonate fuel cells for CO2 separation and segregation by retrofitting existing plants - an analysis of feasible operating windows and first experimental findings, Int. J. Greenh. Gas Control 35 (Apr. 2015) 120–130, https://doi.org/10.1016/j.ijggc.2015.01.012.
[13] F. Yoshiba, Kawagoe 300kW class MCFC/TCG compact system: thermal efficiency and endurance test results, J. Fuel Cell Sci. Technol. 5 (2) (May 2008), https://doi.org/10.1115/1.2784281.
[14] T.A. Barckholtz, K.M. Taylor, S. Narayanan, S. Jolly, H. Ghezel-Ayagh, Molten carbonate fuel cells for simultaneous CO2 capture, power generation, and H2 generation, Appl. Energy 313 (May 2022), https://doi.org/10.1016/j.apenergy.2022.118553.
[15] M. Archetti, E. Audasso, B. Bosio, D. Bove, High temperature fuel cells to reduce CO2 emission in the maritime sector, in: E3S Web of Conferences, EDP Sciences, Jan. 2022, https://doi.org/10.1051/e3sconf/202233404013.
[16] B. Bosio, M. Archetti, E. Audasso, D. Bove, Process analysis of a molten carbonate fuel cell on-board application to reduce vessel CO2 emissions, Chem. Eng. Process. Process Intensif. 190 (Aug) (2023), https://doi.org/10.1016/j.cep.2023.109415.
[17] R. Risso, L. Cardona, M. Archetti, F. Lossani, B. Bosio, D. Bove, A review of On-Board carbon capture and storage techniques: solutions to the 2030 IMO regulations, Energies (Basel) 16 (18) (Sep. 2023), https://doi.org/10.3390/en16186748.
[18] P. Wang, K. Du, H. Yin, D. Wang, Corrosion and Protection of Metallic Materials in Molten Carbonates for Concentrating Solar Power and Molten Carbonate Electrolysis Applications, Elsevier B.V., Sep. 01, 2023, https://doi.org/10.1016/j.corcom.2023.01.003.
[19] S. Frangini, M. Della Pietra, L. Della Seta, C. Paoletti, J. Pedro Pérez-Trujillo, Degradation of MCFC materials in a 81 cm 2 single cell operated under alternated fuel cell/electrolysis modes I n r e v i e w, Front. Energy Res. (2021) [Online]. Available: www.frontiersin.org.
[20] F. Sessa, M. Della Pietra, S. Mataloni, A.B. Muñoz-García, M. Pavone, Structure and dynamics of Li1.24K0.76CO3 molten carbonate electrolyte from molecular simulations with explicit polarization, Phys. Chem. Chem. Phys. 26 (19) (Apr. 2024) 14420–14429, https://doi.org/10.1039/d4cp00805g.
[21] M.A. Murmura, S. Lo Conte, F. Santoni, M. Della Pietra, L. Turchetti, M.C. Annesini, Two-dimensional modeling and experimental investigation of an inverse molten carbonate fuel cell, J. Power Sources 573 (Jul. 2023), https://doi.org/10.1016/j.jpowsour.2023.233103.
[22] T.A. Barckholtz, et al., Experimental and modeling investigation of CO3=/OH– equilibrium effects on molten carbonate fuel cell performance in carbon capture applications, Front. Energy Res. 9 (Jun. 2021), https://doi.org/10.3389/fenrg.2021.669761.
[23] C.W. Lee, et al., Effect of the flow directions on a 100 cm2 MCFC single cell with internal flow channels, Int. J. Hydrogen Energy 41 (41) (Nov. 2016) 18747–18760, https://doi.org/10.1016/j.ijhydene.2016.03.188.
[24] N. Di Giulio, B. Bosio, V. Cigolotti, S.W. Nam, Experimental and theoretical analysis of H2S effects on MCFCs, Int. J. Hydrogen Energy 37 (24) (Jul. 2012) 19329–19336, https://doi.org/10.1016/j.ijhydene.2012.03.086.
[25] S. Lo Conte, S. Mataloni, M. Della Pietra, L. Simonetti, Y. De Pra, M.C. Annesini, DRT-Based electrochemical investigation on the fuel electrode in a molten carbonate electrolysis cell, J. Power Sources 631 (Mar) (2025), https://doi.org/10.1016/j.jpowsour.2025.236197.
[26] J.P. Pérez-Trujillo, F. Elizalde-Blancas, S.J. McPhail, M. Della Pietra, B. Bosio, Preliminary theoretical and experimental analysis of a molten carbonate fuel cell operating in reversible mode, Appl. Energy 263 (Apr) (2020), https://doi.org/10.1016/j.apenergy.2020.114630.
[27] L. Hu, G. Lindbergh, C. Lagergren, Performance and durability of the molten carbonate electrolysis cell and the reversible molten carbonate fuel cell, J. Phys. Chem. C 120 (25) (Jun. 2016) 13427–13433, https://doi.org/10.1021/acs.jpcc.6b04417.
[28] J.P. Perez-Trujillo, F. Elizalde-Blancas, M. Della Pietra, S.J. McPhail, A numerical and experimental comparison of a single reversible molten carbonate cell operating in fuel cell mode and electrolysis mode, Appl. Energy 226 (Sep. 2018) 1037–1055, https://doi.org/10.1016/j.apenergy.2018.05.121.
[29] H. Meskine, V. Albin, M. Cassir, A. Ringuedé, V. Lair, Electrochemical investigations on CO2 reduction mechanism in molten carbonates in view of H2O/CO2 co-electrolysis, Int. J. Hydrogen Energy 46 (28) (Apr. 2021) 14944–14952, https://doi.org/10.1016/j.ijhydene.2020.07.008.
[30] Z. Yang, B. Deng, K. Du, H. Yin, D. Wang, A general descriptor for guiding the electrolysis of CO2 in molten carbonate, Green Energy Environ. 9 (4) (Apr. 2024) 748–757, https://doi.org/10.1016/j.gee.2022.09.011.
[31] D. Monzer, C. Bouallou, Production of synthetic gas by the co-electrolysis of H2O and CO2 in the molten carbonate electrolyzer, Int. J. Hydrogen Energy 52 (Jan. 2024) 152–166, https://doi.org/10.1016/j.ijhydene.2023.03.402.
[32] A. Martsinchyk, et al., Molten carbonate electrolyzer for synthetic fuel generation, J. Power Sources 628 (Feb) (2025), https://doi.org/10.1016/j.jpowsour.2024.235741.

[33] H. Meskine, et al., CO2 electrolysis in a reversible molten carbonate fuel cell: online chromatographic detection of CO, Int. J. Hydrogen Energy 46 (28) (Apr. 2021) 14913–14921, https://doi.org/10.1016/j.ijhydene.2020.08.028.
[34] E. Audasso, K.I. Kim, G. Accardo, H.S. Kim, S.P. Yoon, Investigation of molten carbonate electrolysis cells performance for H2 production and CO2 capture, J. Power Sources 523 (Mar) (2022), https://doi.org/10.1016/j.jpowsour.2022.231039.
[35] L. Hu, G. Lindbergh, C. Lagergren, Electrode kinetics of the Ni porous electrode for hydrogen production in a Molten Carbonate Electrolysis Cell (MCEC), J. Electrochem. Soc. 162 (9) (2015) F1020–F1028, https://doi.org/10.1149/2.0491509jes.
[36] A. Zhadan, V. Sarou-Kanian, L. Del Campo, L. Cosson, M. Malki, C. Bessada, Transport properties in molten carbonates: self-diffusion and conductivity measurements at high temperature, Int. J. Hydrogen Energy 46 (28) (Apr. 2021) 15059–15065, https://doi.org/10.1016/j.ijhydene.2020.06.294.
[37] E. Gürbüz, E. Grépin, A. Ringuedé, V. Lair, M. Cassir, Significance of Molten Hydroxides with or Without Molten Carbonates in High-Temperature Electrochemical Devices, Frontiers Media S.A, Apr. 29, 2021, https://doi.org/10.3389/fenrg.2021.666165.
[38] T. Kojima, Y. Miyazaki, K. Nomura, K. Tanimoto, Electrical conductivity of molten li[sub 2]CO[sub 3]–X[sub 2]CO[sub 3] (X: na, K, Rb, and Cs) and Na[sub 2]CO[sub 3]–Z[sub 2]CO[sub 3] (Z: k, Rb, and Cs), J. Electrochem. Soc. 154 (12) (2007) F222, https://doi.org/10.1149/1.2789389.
[39] K.I. Kim, et al., In situ electrolyte replenishment with atmospheric pressure-chemical/electrochemical vapour deposition for molten carbonate fuel cells, Chem. Eng. J. 476 (Nov. 2023), https://doi.org/10.1016/j.cej.2023.146663.
[40] C.Y. Yuh, J.R. Selman, The polarization of molten carbonate fuel cell electrodes: II . Characterization by AC impedance and response to current interruption, J. Electrochem. Soc. 138 (12) (Dec. 1991) 3649–3656, https://doi.org/10.1149/1.2085474.
[41] M. Yoshikawa, A. Bodén, M. Sparr, G. Lindbergh, Experimental determination of effective surface area and conductivities in the porous anode of molten carbonate fuel cell, J. Power Sources 158 (1) (Jul. 2006) 94–102, https://doi.org/10.1016/j.jpowsour.2005.09.038.
[42] F. Santoni, et al., Accurate in-operando study of molten carbonate fuel cell degradation processes -part I: physiochemical processes individuation, Electrochim. Acta 291 (Nov. 2018) 343–352, https://doi.org/10.1016/j.electacta.2018.08.100.
[43] B. Bosio, N. Di Giulio, S.W. Nam, A. Moreno, An effective semi-empiric model for MCFC kinetics: theoretical development and experimental parameters identification, Int. J. Hydrogen Energy 39 (23) (Aug. 2014) 12273–12284, https://doi.org/10.1016/j.ijhydene.2014.04.119.
[44] L. Barelli, G. Bidini, G. Cinti, J. Milewski, High temperature electrolysis using molten carbonate electrolyzer, Int. J. Hydrogen Energy 46 (28) (Apr. 2021) 14922–14931, https://doi.org/10.1016/j.ijhydene.2020.07.220.
[45] S. Koomson, S.H. Bae, K.M. Kim, C.G. Lee, Effect of temperature on the electrode overpotential of molten carbonate electrolysis and fuel cells with inert-gas step addition method, J. Electroanal. Chem. 950 (Dec) (2023), https://doi.org/10.1016/j.jelechem.2023.117844.
[46] S.H. Clarke, A.L. Dicks, K. Pointon, T.A. Smith, A. Swann, Catalytic Aspects of the Steam Reforming of Hydrocarbons in Internal Reforming Fuel Cells, 1997.
[47] L. Hu, G. Lindbergh, C. Lagergren, Operating the nickel electrode with hydrogen-lean gases in the molten carbonate electrolysis cell (MCEC), Int. J. Hydrogen Energy 41 (41) (Nov. 2016) 18692–18698, https://doi.org/10.1016/j.ijhydene.2016.06.037.
[48] B. Smith R J, M. Loganathan, M.S. Shantha, A review of the water gas shift reaction kinetics, Int. J. Chem. React. Eng. 8 (1) (Jun. 2010), https://doi.org/10.2202/1542-6580.2238.